atmosphere

MDPI

Article

Investigation of Secondary Organic Aerosol Formation during O_3 and $PM_{2.5}$ Episodes in Bangkok, Thailand

Pornpan Uttamang [1], Parkpoom Choomanee [2,*], Jitlada Phupijit [2,3], Surat Bualert [2] and Thunyapat Thongyen [4]

[1] Environmental Technology Program, Faculty of Science, Maejo University, Chiang Mai 50290, Thailand; pornpan_um@mju.ac.th
[2] Department of Environmental Science, Faculty of Environment, Kasetsart University, Bangkok 10900, Thailand; jitlada@rimes.int (J.P.); surat.b@ku.ac.th (S.B.)
[3] Regional Integrated Multi-Hazard Early Warning System, AIT Campus, Pathumthani 12120, Thailand
[4] Department of Environmental Technology and Management, Faculty of Environment, Kasetsart University, Bangkok 10900, Thailand; thunyapat.t@ku.ac.th
* Correspondence: parkpoom.choom@ku.th

Abstract: In Bangkok, the megacity of Thailand, concentrations of fine particulate matter ($PM_{2.5}$) have often exceeded the National Ambient Air Quality standards. During severe smog events over Bangkok, the air quality has exhibited moderate to unhealthy atmospheric conditions, according to the air quality index of the United States. To investigate the formation of secondary organic aerosols (SOA), a field campaign to estimate secondary organic carbon (SOC) in Bangkok using the EC tracer method was conducted in January 2021, when the concentrations of $PM_{2.5}$ were high. The monthly period was classified into three pollution groups, including high pollution, high PM, and low pollution events. The study showed that the correlations between $PM_{2.5}$ and O_3 were negative during both the daytime and night-time. The OC/EC ratios varied from 4.32 to 5.43, while the moderate OC/EC values implied that fossil fuel combustion was the major carbonaceous aerosol in Bangkok. The EC tracer-estimated SOC and POC showed that SOC contributed between 32.5 and 46.4% to OC, while the highest SOC contribution occurred during the low pollution event. The heightened formation of SOA during the low pollution event was perhaps owing to the levels of oxides of nitrogen (NO_x). Since Bangkok is more likely to have a NO_x-rich photochemical reaction regime, an increase in the NO_x level tended to decrease the SOA yield ([NO_x] was 21.6 ppb, 20.8 ppb, and 17.1 ppb during the high pollution, high PM, and low pollution events, respectively). Together with the high humidity and high light intensity during the low pollution event, the SOA formation was enhanced. Even though the driving factors of SOA formation over Bangkok remain unclear, the results of this study reveal the significance and urgency of local actions to reduce NO_x and O_3 towards more habitable and sustainable urban environments.

Keywords: secondary organic aerosol (SOA); $PM_{2.5}$; ozone; urban air quality

check for updates

Citation: Uttamang, P.; Choomanee, P.; Phupijit, J.; Bualert, S.; Thongyen, T. Investigation of Secondary Organic Aerosol Formation during O_3 and $PM_{2.5}$ Episodes in Bangkok, Thailand. *Atmosphere* **2023**, *14*, 994. https://doi.org/10.3390/atmos14060994

Academic Editor: Antonio Donateo

Received: 1 May 2023
Revised: 31 May 2023
Accepted: 5 June 2023
Published: 7 June 2023

1. Introduction

In the past few years, Bangkok, the megacity of Thailand, has experienced high concentrations of fine particulate matter ($PM_{2.5}$). According to the 2020 report on the quality of the environmental state, the annual average $PM_{2.5}$, ranging from 28.6 to 31.5 μg m^{-3} in Bangkok during 2012–2019, often exceeded the National Ambient Air Quality Standards (NAAQS) (annual $PM_{2.5}$ standard is 25 μg m^{-3}) [1]. High concentrations of $PM_{2.5}$ normally occur in the winter (October to February) and in the transitional period between the winter and summer (February to May) [2,3]. In March 2023, the air quality index value of the United States (US AQI) for Bangkok ranged from a moderate level (59) to an unhealthy level (170), with the daily average $PM_{2.5}$ ranging from 40 to 81 μg m^{-3} [4]. Furthermore, the comparison between the yearly average concentrations of ultrafine particles ($PM_{0.1}$) in large cities in Southeast Asia showed that Bangkok had very high concentrations of $PM_{0.1}$ [5].

Absorbed through the respiratory and circulatory systems, $PM_{2.5}$ can exert adverse effects on human health, such as aggravated asthma, pulmonary inflammation, cardiopulmonary effects, and the premature death of people with heart or lung disease [6,7]. Biomass burning and fossil fuel combustion from vehicles are considered to be the major emission sources of pollutants, such as particulate matter (PM), ozone (O_3), oxide of nitrogen (NO_x), and carbon monoxide (CO) in Bangkok [5,8–10].

Fine PM ($PM_{2.5}$) can be formed from various chemical compounds, such as organic carbon (OC), elemental carbon (EC), metals, and inorganic species [10,11]. In Thailand, the major chemical compositions in $PM_{2.5}$ are OC, anions (the sum of Cl^-, NO_3^-, SO_4^{2-}), cations (the sum of $Na^+, NH_4^+, K^+, Ca^{2+}, Mg^{2+}$), sulfate, and nitrate [12]. OC in aerosols can be classified into primary organic carbon (POC) and secondary organic carbon (SOC). POC originates from, or is directly emitted from, emission sources, whereas SOC is generated from atmospheric chemical mechanisms, such as gas-particle conversion or oxidation processes in the atmosphere [12,13]. To estimate the contribution of SOC to the $PM_{2.5}$ concentration, the EC tracer method proposed by Turpin and Huntzicker (1991) [14] has been widely used [15–17]. Secondary organic aerosols (SOA) can be estimated by multiplying the SOC concentration by the organic mass-to-OC conversion factor [18]. There are several processes in the formation of SOA in the atmosphere. The oxidation of hydrocarbon (HC) by hydroxyl radicals (OH) and O_3 is considered a major mechanism for the daytime formation of SOA. Although the formation of OH and O_3 are suppressed during night-time, the oxidation of HC by O_3 and nitrate radicals (NO_3) is the major night-time process that creates SOA [19]. Previous studies have attempted to investigate the correlation between O_3 and SOA in many countries, but in Asia, studies have mainly focused on China. In the related literature, a positive correlation between $PM_{2.5}$ and O_3 was reported during a hot season, since O_3, a strong oxidiser, enhanced the formation of secondary particulate matter [20,21]. In Beijing–Tianjin–Hebei, China, a 31% O_3 reduction decreased SOA by approximately 30% [22]. In the Yangtze River Delta, China, the increased surface level of O_3 moderately enhanced the level of SOC [23]. During a cold season in China, a negative correlation between O_3 and $PM_{2.5}$ was found since the high concentration of $PM_{2.5}$ attenuated sunlight, reduced the photolysis rate, and suppressed O_3 formation [20]. In addition, the reactive uptake of hydroperoxy radicals (HO_2) and nitrogen oxides (NO_2, NO_3, and N_2O_5) can inhibit the reaction between HO_2 and NO, thus reducing O_3 formation [24].

To analyse the possible causes of the SOA enhancement and the atmospheric conditions and chemical reactions that raised $PM_{2.5}$ levels over Bangkok, a field campaign (hereinafter called the SOC campaign) was conducted to measure O_3, $PM_{2.5}$, PM_{10}, and meteorological variables in January 2021 via the microclimate and air pollutant monitoring tower located at Kasetsart University, Bangkok. The observations were conducted at 30 m above ground level (agl), with the lowest observation level at the tower. The concentrations of POC, SOC, OC, and EC were estimated using the EC tracer method. The correlations between the chemical species, the ratio of $PM_{2.5}$ to PM_{10}, and the ratio of OC to EC were analysed. Previous studies have shown that the $PM_{2.5}/PM_{10}$ ratio could reveal the emission sources and processes of particles in the atmosphere [25–29]. A low $PM_{2.5}/PM_{10}$ ratio indicates that coarse particles that originate from natural emission sources (e.g., dust or sand dust from long-distance transport) are dominant, whereas a high $PM_{2.5}/PM_{10}$ ratio suggests that fine particles predominate due to anthropogenic sources and secondary particulate formation [25–28]. Several studies (e.g., [30–33]) have reported that the major emission sources could be indicated by the OC/EC ratio. An OC/EC ratio ranging from 1.0 to 4.2 suggests that vehicles are the major source of aerosols. OC/EC ratios ranging from 2.5 to 10.5, 3.8 to 13.2, and 32.9 to 81.6 reveal coal combustion, biomass combustion, and cooking as the main emission sources, respectively [34]. A better understanding of the origin, atmospheric fate, and impact of SOA may enable SOA to be used as an additional metric for monitoring urban air quality in megacities.

2. Materials and Methods

2.1. Sampling Site

The observations in this study were conducted during January 2021 via the microclimate and air pollutant monitoring tower located at Kasetsart University (KU tower), Bangkok, Thailand (latitude: 13.854529N, longitude: 100.570012E) (Figure 1). This study area is considered an urban area, surrounded by commercial buildings, residential buildings, and traffic routes. There is an elevated tollway (Uttaraphimuk elevated tollway), with a high traffic volume of approximately 80,000 vehicles per day [35], located approximately 400 m away on the east of the KU tower. The land-use and land-cover types within a radius of 5 km from the KU tower were classified as buildings and residential communities (94%), roads (4%), water bodies, and others (2%) [9].

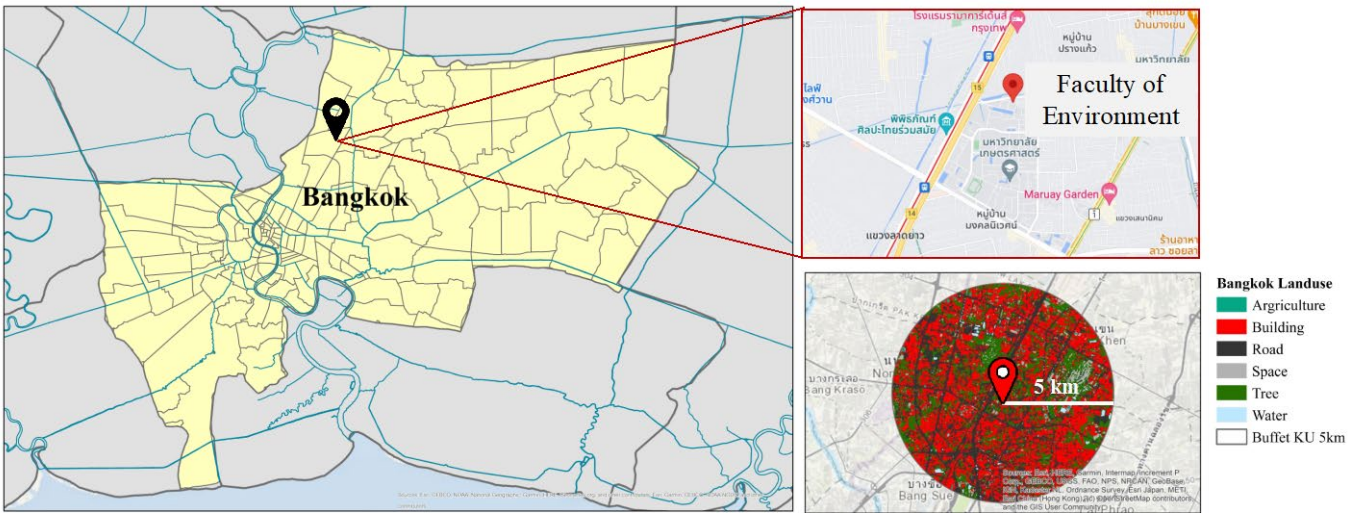

Figure 1. Microclimate and air pollutant monitoring tower located at Kasetsart University (KU tower), Bangkok, Thailand, and land-use and land-cover types around the study area.

Bangkok has a tropical climate where, during the local winter season (October to February), the northeast monsoon wind brings a dry air mass from China and Mongolia, thus resulting in dry and cool weather. February to May is the transitional period from the northeast monsoon to the southwest monsoon. During the local summer season (from February to May), the weather is hot or very hot. During the months from May to October, a southwest monsoon wind with high moisture travels from the Indian Ocean to this region, resulting in the rainy season [2,3]. During the dry seasons, the air pollution levels in Bangkok are normally high due to the northeast monsoon winds that travel past high pollution areas (i.e., high traffic volume, commercial areas, high population density areas, and high biomass burning areas) and carry the pollution to Bangkok [10,36]. This is especially the case during December to February, which can be considered the smog season in Bangkok [37]. On the other hand, during the wet season, the air pollution levels in Bangkok are low due to dilution from the clean marine air masses and rainy washout. Therefore, our study focuses on examining carbonaceous aerosols during January due to the larger concentrations.

2.2. Data Collection

The hourly concentrations of $PM_{2.5}$, PM_{10}, O_3, and NO_x and meteorological parameters, including wind speed (WS), wind direction (WD), temperature (T), relative humidity (RH), and light intensity, were measured at 30 m agl. The hourly concentrations of $PM_{2.5}$ and PM_{10} were measured using a tapered element oscillating microbalance (TEOM) technique (1405-DF TEOMTM Continuous Dichotomous Ambient Air Monitor; Thermo Fisher Scientific Inc., Waltham, MA, USA). The concentrations of O_3 and NO_x were detected using

an ultraviolet (UV) photometer O_3 analyser (49i Ozone analyser; Thermo Fisher Scientific Inc., Waltham, MA, USA) and a NO_x analyser (49i Ozone analyser; Thermo Fisher Scientific Inc., Waltham, MA, USA), respectively. For the meteorological parameters, the WS and WD were measured using a wind cup anemometer and a wind vane (LSI LASTEM, DNA827, Milano, Italy). The T and RH were measured using a thermo-hygrometer (LSI LASTEM, DMA867 and DMA875). The light intensity (UV wavelength 300–400 nm) was measured using a spectroradiometer 350–2050 nm (EKO instruments, MS700, Tokyo, Japan).

To estimate the SOC, $PM_{2.5}$ were continuously collected on a quartz microfiber filter of 37 mm in diameter (TE-QMA-37, Tisch Environmental Inc., OH, USA) using an area dust monitor (ADR1500; Thermo Fisher Scientific Inc., Waltham, MA, USA) with a flow rate of 1.52 L/min. The quartz filters were heated at 550 °C for one hour before placement in the area dust monitor. The samples were collected twice a day, including from 08:00 to 19:00 (daytime) and from 20:00 to 07:00 (night-time). The loaded filters were preserved at approximately 4 °C to prevent the evaporation of chemical species.

2.3. OC and EC Contaminant Analysis and Estimation of POC and SOC

To analyse the OC and EC components in $PM_{2.5}$, a thermal–optical method (Sunset laboratory carbon analyser with detection limits of 0.2 μg cm^{-2} for OC and 0.40 μg cm^{-2} for EC) with the IMPROVE protocol [5,10,38,39] was used. The analyser was calibrated prior to use with a sucrose solution standard (N = 5, R^2 = 0.99). The loaded sample quartz filter was cut to a size of 1.5 cm^2 and exposed stepwise to temperature. The OC component analysis was conducted in a pure Helium (He) atmosphere, followed by four selected temperature steps at 140 °C, 290 °C, 480 °C, and 580 °C to analyse OC1, OC2, OC3, and OC4, respectively. The analysis of the EC components was conducted in a mixed 2% O_2 and 98% He atmosphere, followed by three selected temperature steps at 580 °C for EC1, 740 °C for EC2, and 840 °C for EC3 analysis. The total OC (OC_{total}) and EC (EC_{total}) were calculated using the following equations:

$$OC_{total} = OC1 + OC2 + OC3 + OC4 + PC$$

$$EC_{total} = EC1 + EC2 + EC3 - PC$$

where PC is the split point between those phases and is automatically set when the measured optical signal returns to the baseline [40] to minimise the uncertainty, due to the formation of pyrolytic carbon (PC) from the OC into the thermally stable form having similarity with EC [41].

We estimated the concentrations of POC and SOC in $PM_{2.5}$ by performing the EC tracer method, which has been widely used to estimate the partitioning of measured particulate OC into primary and secondary fractions [10,14,42,43], as follows:

$$POC = EC \times \left(\frac{OC}{EC}\right)_{pri} + b$$

$$SOC = OC_{total} - POC$$

where $\left(\frac{OC}{EC}\right)_{pri}$ is the ratio of OC to EC in the primary emissions. In this study, the lowest 10% of $\left(\frac{OC}{EC}\right)$ was considered $\left(\frac{OC}{EC}\right)_{pri}$ [17,23,44]. The OC_{total} measured the particulate OC, and b was the interception from the OC vs. EC scatter plot, which was interpreted as the POC from activities other than the combustion processes, such as road dust resuspension, biogenic emissions, and fuel and solvent evaporation [15,45].

Furthermore, the quantitative criteria to select the OC and EC data in order to determine $\left(\frac{OC}{EC}\right)_{pri}$ were not clear, and $\left(\frac{OC}{EC}\right)_{pri}$ had diurnal and seasonal variations [43,46].

3. Results and Discussion

3.1. Classification of Pollution Events

During the SOC campaign, the hourly maximum, minimum, and average concentrations at 30 m agl were estimated at 141.9 μg m^{-3}, 12.0 μg m^{-3}, and 49.69 ± 25.61μg m^{-3} for $PM_{2.5}$; 177.5 μg m^{-3}, 18.5 μg m^{-3}, and 69.80 ± 31.43 μg m^{-3} for PM_{10}; and 94.2 ppb, 11.6 ppb, and 39.5 ± 19.0 ppb for O_3, respectively. The ratio of $PM_{2.5}/PM_{10}$ in this study ranged from 0.42 to 0.89, and the average was 0.70 ± 0.08 (Table 1).

Table 1. The hourly maximum, minimum, and average (+ standard deviation [SD]) values of $PM_{2.5}$, PM_{10}, O_3, and $PM_{2.5}/PM_{10}$ during the SOC campaign.

Species	Maximum	Minimum	Average ± SD
$PM_{2.5}$ (μg m^{-3})	141.88	11.97	49.69 ± 25.61
PM_{10} (μg m^{-3})	177.46	18.53	69.80 ± 31.43
O_3 (ppb)	94.22	11.6	39.45 ± 18.96
$PM_{2.5}/PM_{10}$	0.89	0.42	0.70 ± 0.08

The study period was classified into three events, including high pollution, high particulate matter (PM), and low pollution events. During the high pollution event, the daily concentrations of $PM_{2.5}$ were greater than 50 μg m^{-3} (Thailand's National Ambient Air Quality Standards (NAAQS) of 50 μg m^{-3} for daily-average $PM_{2.5}$), and the hourly concentrations of O_3 were greater than 77.4 ppb. Since the hourly O_3 concentrations (11.6 to 94.22 ppb) were within the standard (the NAAQS of Thailand for the hourly O_3 is 100 ppb), we, therefore, applied the hourly average concentration of O_3 + 2SD as the O_3 threshold (77.4 ppb). During the high PM event, the daily average concentrations of $PM_{2.5}$ exceeded the standard, while the hourly concentrations of O_3 were at the threshold. When the daily average concentrations of $PM_{2.5}$ and the hourly concentrations of O_3 were at the threshold, the atmosphere was considered to be a low pollution event. The criteria to classify the atmospheric conditions are summarised in Table 2.

Table 2. The criteria for atmospheric pollution conditions classification during the SOC campaign in January 2022.

Episode	$PM_{2.5}$ (μg m^{-3})	O_3 (ppb)	Day of the Month	Total Day
High pollution	>50	>77.4	16 to 20 and 23	6
High PM	>50	≤77.4	4, 13 to 15, 21 to 22, 24, and 29 to 31	10
Low pollution	≤50	≤77.4	1 to 3, 5 to 12, and 25 to 28	15

During the study period, the 24 h averages of $PM_{2.5}$ exceeded the standard for 15 days (4, 13 to 24, and 30 to 31 January), with concentrations ranging from 52.4 to 95.2 μg m^{-3}. During those days, the daily average concentrations of PM_{10} ranged from 69.9 to 119.5 μg m^{-3}. The hourly O_3 concentrations during the study period were below the standard, with concentrations ranging from 11.6 to 94.2 ppb. High concentrations of O_3 (above 77.4 ppb) were observed from 16 to 20 January and on 23 January. Therefore, from 16 to 20 and on 23 January, the atmospheric condition was classified as a high pollution event (high $PM_{2.5}$ and O_3), with daily average $PM_{2.5}$ and PM_{10} and hourly average O_3 concentrations of 74.4 ± 16.3 μg m^{-3}, 97.8 ± 17.8 μg m^{-3}, and 59.8 ± 23.7 ppb, respectively. The atmospheric conditions during 4, 13 to 15, 21 to 22, 24, and 29 to 31 January were considered high PM events, with daily average $PM_{2.5}$ and PM_{10} concentrations of 70.4 ± 16.3 μg m^{-3} and 96.9 ± 18.1 μg m^{-3}, respectively, and an hourly average O_3 concentration of 36.5 ± 15.3 ppb. The atmospheric condition from 1 to 3, 5 to 12, and 25 to 28 January was classified as a low pollution event, with daily average $PM_{2.5}$ and PM_{10} and hourly O_3 concentrations of 39.6 ± 12.4 μg m^{-3}, 56.3 ± 14.8 μg m^{-3}, and 33.2 ± 12.4 ppb, respectively. The daily

average $PM_{2.5}$ and PM_{10} during the high pollution and high PM events were in the range of those observed from megacities in China, such as Beijing (87.0 μg m^{-3} for $PM_{2.5}$ and 109.4 μg m^{-3} for PM_{10}), Shanghai (56.1 μg m^{-3} for $PM_{2.5}$ and 79.9 μg m^{-3} for PM_{10}), and Guangzhou (51.6 μg m^{-3} for $PM_{2.5}$ and 72.5 μg m^{-3} for PM_{10}) [47] and those observed over the Indo-Gangetic Plain of India ($PM_{2.5}$ ranging from 66 to 98 μg m^{-3}) [48]. The hourly average O_3 during the high pollution event was comparable to the hourly average O_3 in Beijing (52.5 ppb), Shanghai (56.1 ppb), and Guangzhou (58.3 ppb). The daily average ratios of $PM_{2.5}/PM_{10}$ were 0.73, 0.71, and 0.67 during the high pollution, high PM, and low pollution events, respectively. The high $PM_{2.5}/PM_{10}$ ratio suggested that both anthropogenic emissions and the formation of secondary particulate matter enhanced the PM levels over the study area [25–28]. Figure 2 illustrates a time series of hourly $PM_{2.5}$, PM_{10}, O_3, and $PM_{2.5}/PM_{10}$ ratios during the high pollution, high PM, and low pollution events during the SOC campaign in January 2021.

The meteorological observations made during the high pollution, high PM, and low pollution events are shown in Table 3 and Figure 3. In January, the winds often originated from the northeast, with the average WS ranging from 1.72 to 2.00 m s^{-1}. The average WS was high (2.00 ± 1.22 m s^{-1}) during the low pollution event and low (1.72 ± 1.06 m s^{-1}) during the high PM event.

Table 3. Meteorological factors during the high pollution, high PM, and low pollution events.

Parameters	Events	Maximum	Minimum	Mean
Wind Speed (m s^{-1})	High pollution	5.57	0.16	1.84 ± 1.21
	High PM	7.10	0.10	1.72 ± 1.06
	Low pollution	6.83	0.04	2.00 ± 1.22
Temperature (°C)	High pollution	31.99	18.78	25.12 ± 3.21
	High PM	32.01	16.43	25.81 ± 3.43
	Low pollution	33.09	16.74	26.13 ± 3.47
Relative Humidity (%)	High pollution	100.00 (34) *	32.67 (11)	56.83 ± 18.10 (19 ± 6)
	High PM	100.00 (34)	29.32 (10)	50.27 ± 12.59 (17 ± 4)
	Low pollution	100.00 (36)	34.42 (12)	57.35 ± 16.08 (20 ± 6)
Light Intensity ** (wm^{-2} μm^{-1})	High pollution	212.3	0.0	74.3 ± 61.8
	High PM	234.7	0.0	76.5 ± 62.4
	Low pollution	235.7	0.0	76.5 ± 66.0

Note: * absolute humidity (g m^{-3}) at 1010 hPa. ** UV wavelength (300–400 nm) measured between 8:00 and 19:00.

Overall, the average T value varied between 25.12 and 26.13 °C. The average RH levels were 56.8 ± 18.10, 50.27 ± 12.59, and 57.35 ± 16.08% during the high pollution, high PM, and low pollution events, respectively. The average light intensity measured from 8:00 to 19:00 during the high pollution event was 74.3 ± 61.8 wm^{-2} μm^{-1}, during the high PM event was 76.5 ± 62.4 wm^{-2} μm^{-1}, and during the low pollution event was 76.5 ± 66.0 wm^{-2} μm^{-1}. The results reveal possible causes of the formation, accumulation, and dispersion of the pollution during the SOC due to meteorological factors. For example, high air pollution levels decreased solar radiation, which could affect photochemical reactions in the atmosphere. However, the meteorological factors alone could not fully account for the high pollutant concentrations during the high pollution event.

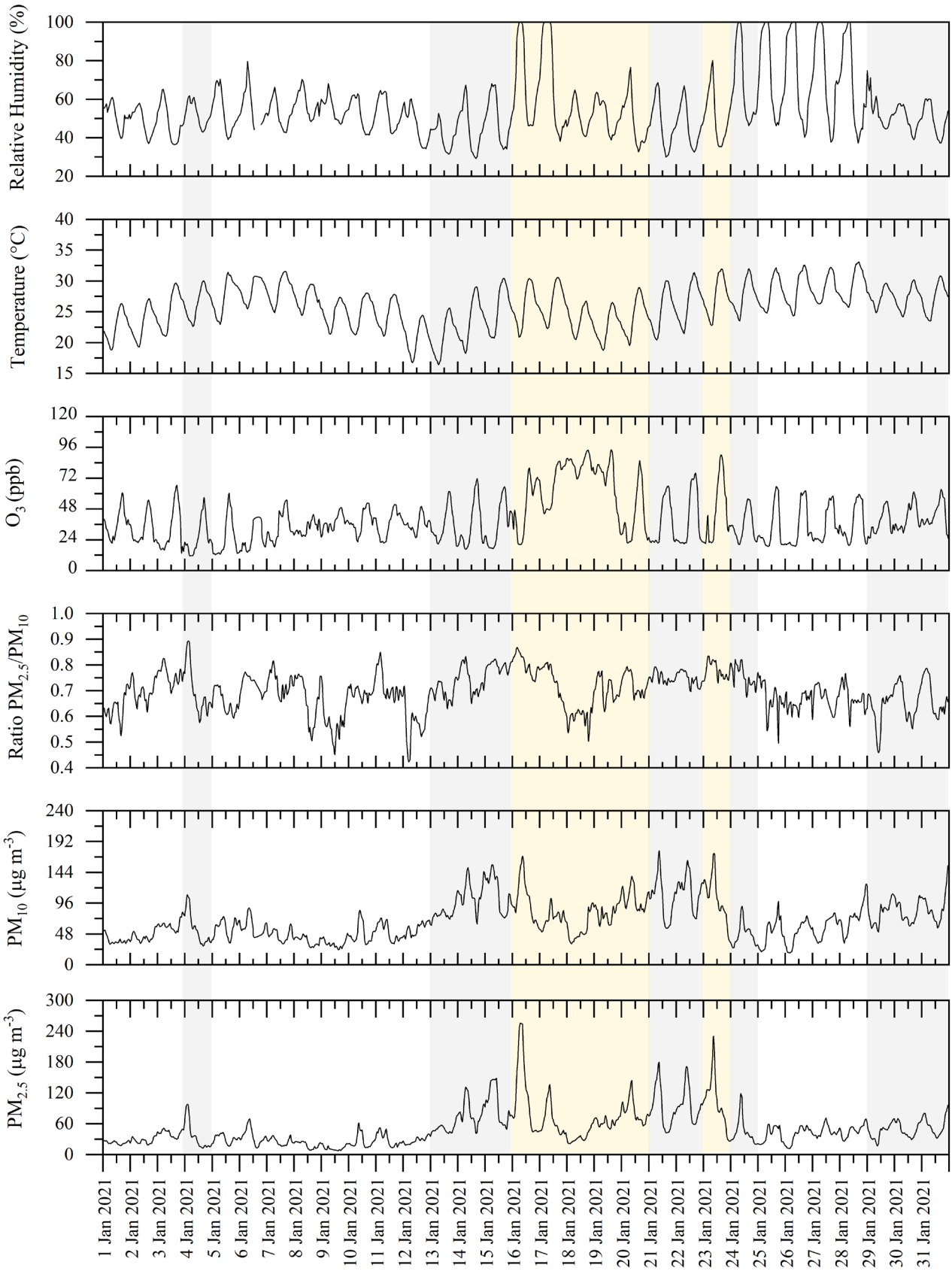

Figure 2. Time series of hourly (**a**) $PM_{2.5}$ (μg m^{-3}), (**b**) PM_{10} (μg m^{-3}), (**c**) O_3 (ppb) concentrations, and (**d**) $PM_{2.5}/PM_{10}$ ratios during 1–31 January 2021. Yellowish and greyish bands refer to the high pollution and high PM events, respectively.

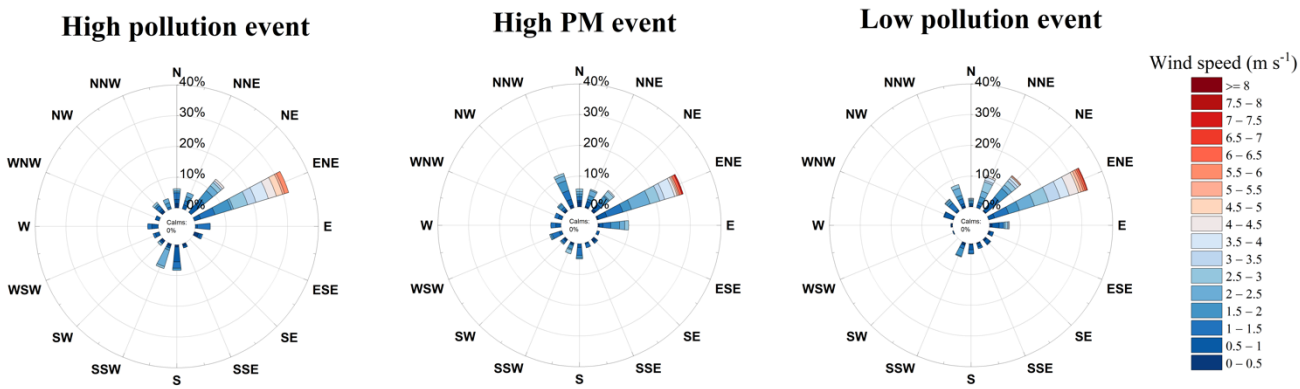

Figure 3. Wind rose diagrams during the high pollution, high PM, and low pollution events at 30 m agl at the KU tower.

3.2. Correlation between $PM_{2.5}$ and O_3

The correlations between $PM_{2.5}$ and O_3 during the three events are shown in Table 4. This study revealed that $PM_{2.5}$ was inversely correlated with O_3. The strongest negative correlation between $PM_{2.5}$ and O_3 occurred during the high pollution event, with a coefficient of correlation (r) value of −0.64, followed by the high PM (r = −0.38) and low pollution (r = −0.18) events. The correlations between $PM_{2.5}$ and O_3 were also analysed separately during the daytime and night-time since the formation process of PM differs between these times.

Table 4. The average total, daytime, and night-time $PM_{2.5}$, PM_{10}, and O_3 concentrations and $PM_{2.5}/PM_{10}$ ratio and correlations between $PM_{2.5}$ and O_3 (r($PM_{2.5}$-O_3)), OC, EC, OC/EC ratio, POC, SOC, and POC/SOC ratio during the high pollution, high O_3, high PM, and low pollution events.

Events	$PM_{2.5}$ (μg m^{-3})	PM_{10} (μg m^{-3})	O_3 (ppb)	$PM_{2.5}/PM_{10}$	*r* ($PM_{2.5}$-O_3)	OC (μg m^{-3})	EC (μg m^{-3})	OC/EC	POC (μg m^{-3})	SOC (μg m^{-3})	SOC/POC
Total											
High pollution	78.3 ± 48.8	85.9 ± 30.1	59.8 ± 23.7	0.73	−0.64	64.92 ± 20.72	14.31 ± 7.67	4.54	41.72 ± 22.36	23.20 ± 9.29	0.56
High PM	65.2 ± 34.5	88.1 ± 32.3	36.5 ± 15.3	0.71	−0.38	75.38 ± 28.38	17.47 ± 9.21	4.32	50.92 ± 26.84	24.46 ± 11.68	0.48
Low pollution	31.4 ± 14.0	50.8 ± 17.2	33.2 ± 12.4	0.67	−0.18	50.75 ± 12.98	9.34 ± 3.92	5.43	27.21 ± 11.44	23.54 ± 7.46	0.86
Daytime											
High pollution	72.3 ± 51.2	81.8 ± 33.1	61.7 ± 23.0	0.70	−0.43	61.57 ± 23.68	12.42 ± 5.50	4.96	36.18 ± 16.02	25.38 ± 8.18	0.70
High PM	59.9 ± 36.5	82.1 ± 31.0	44.9 ± 15.4	0.69	−0.40	61.73 ± 17.34	12.14 ± 4.19	5.08	35.39 ± 12.20	26.34 ± 7.73	0.74
Low pollution	31.8 ± 15.6	51.4 ± 17.2	39.0 ± 12.9	0.65	−0.17	46.42 ± 9.29	8.32 ± 3.47	5.58	24.26 ± 10.10	22.16 ± 7.15	0.91
Night-time											
High pollution	76.2 ± 46.9	82.9 ± 29.1	52.3 ± 24.8	0.74	−0.64	68.27 ± 18.90	16.21 ± 9.52	4.21	47.25 ± 27.74	21.03 ± 10.56	0.44
High PM	71.5 ± 31.0	95.0 ± 32.5	26.8 ± 7.4	0.75	−0.27	89.04 ± 31.41	22.80 ± 9.92	3.91	66.45 ± 28.92	22.59 ± 14.85	0.34
Low pollution	30.8 ± 11.9	50.1 ± 17.3	26.7 ± 7.8	0.70	−0.37	55.09 ± 15.11	10.35 ± 4.24	5.32	30.17 ± 12.35	24.92 ± 7.78	0.83

The daytime correlations were −0.43, −0.40, and −0.17 during the high pollution, high PM, and low pollution events, respectively. The attenuation of sunlight by air pollution appeared to cause the negative correlations between $PM_{2.5}$ and O_3 [20]. The negative correlation was stronger during the high pollution and high PM events than during the low pollution event, with a high concentration of O_3, a strong oxidiser, occurring during the high pollution event. The negative correlations between $PM_{2.5}$ and O_3 also occurred at night, with the strongest negative correlation (r = −0.64) being detected during the high pollution event, followed by the low pollution (r = −0.37) and high PM (r = −0.27) events. A negative correlation between O_3 and chemical species is often expected during night-time. At night, O_3 can react with NO, NO_2, and HC to generate NO_2, NO_3, and ozonides, respectively, even though the formation of O_3 is suppressed. Therefore, the O_3 concentration always declines during night-time. To clarify the possible chemical pathways of O_3 and SOA during night-time, the contributions of OC, EC, POC, and SOC are discussed in Section 3.3.

3.3. Temporal Patterns of OC, EC, POC, and SOC

3.3.1. Identification of Emission Sources

For an in-depth $PM_{2.5}$ analysis, the temporal changes in OC, EC, POC, and SOC according to the high pollution, high PM, and low pollution events are presented in Table 4. The $\left(\frac{OC}{EC}\right)_{pri}$ values were determined from the whole data (January data set). The average OC concentrations during the daytime (night-time) varied from 34.0 to 92.1 (44.6 to 95.2) μg m^{-3} during the high pollution event, 43.0 to 89.2 (31.8 to 143.3) μg m^{-3} during the high PM event, and 26.6 to 63.4 (29.6 to 81.5) μg m^{-3} during the low pollution event. The EC concentrations in this study during the daytime (night-time) ranged from 6.0 to 19.1 μg m^{-3} (6.7 to 32.7 μg m^{-3}) during the high pollution event, 5.2 to 17.3 μg m^{-3} (8.0 to 34.1 μg m^{-3}) during the high PM event, and 3.5 to 19.3 μg m^{-3} (3.4 to 17.7 μg m^{-3}) during the low pollution event. While the OC concentrations from our study are comparable to the OC concentrations estimated at Patiala, India during the daytime (ranging from 10 to 119 μg m^{-3}) and night-time (ranging from 15 to 190 μg m^{-3}), the EC concentrations from our study were higher than those reported over Patiala (3.1 to 11.2 μg m^{-3} during the daytime and 3.5 to 12.8 μg m^{-3} during the night-time) [45]. The average OC and EC concentrations during the night-time were usually higher than those during the daytime. In this study, the percentage differences between OC (EC) during the night-time and daytime during the high pollution, high PM, and low pollution events were approximately 9.8 % (23.4%), 30.7% (46.8%), and 15.7% (19.6%), respectively. The OC/EC ratios were 4.54, 4.32, and 5.43 during the high pollution, high PM, and low pollution events, respectively. The OC/EC ratios in this study were comparable to those in Beijing (4.88), Langfang (4.42), and Tianjin (4.22), China [34] and Delhi (4.24 to 5.66), India [49] but were higher than the mean OC/EC at Varanasi, India (3.9). The moderate OC/EC values implied that fossil fuel combustion (i.e., from traffic) was the major carbonaceous aerosol in Bangkok [34,45].

3.3.2. Estimation of Primary and Secondary Organic Carbon Concentrations

Based on the EC tracer method, the concentrations of POC and SOC during the three events were estimated. During the high pollution event, the average POC and SOC concentrations were 41.72 ± 22.36 μg m^{-3} and 23.20 ± 9.29 μg m^{-3} (Table 4), with their contributions to OC comprising 64.3% and 35.7%, respectively (Figure 4). During the high PM event, the average POC and SOC concentrations were 50.92 ± 26.84 μg m^{-3} and 24.46 ± 11.68 μg m^{-3}, which contributed 67.6% and 32.5% to OC, respectively. During the low pollution event, the average POC and SOC concentrations were 27.21 ± 11.44 μg m^{-3} and 23.54 ± 7.46 μg m^{-3}, which accounted for 53.6% and 46.4% of the OC, respectively. Most strikingly, during the low pollution event, SOC and POC contributed to the OC mass equally, and the formation of SOA was heightened. The POC and SOC concentrations from our study were higher than those over northern Europe during a highly processed PM pollution event (POC ranged from 2.2 to 3.7 μg m^{-3} and SOC was 3.3 ± 0.1 μg m^{-3}) [42] and the annual average POC and SOC concentrations over Delhi, India (POC and SOC were 17.0 ± 9.7 and 16.7 ± 9.2 μg m^{-3}, respectively) [50] but were similar to those from Delhi (approximately 50%) [49].

The POC/SOC and OC/EC ratios were separately analysed during the daytime and night-time. SOA formation during the daytime is mainly driven by O_3 [23]; therefore, the OC/EC and SOC/POC ratios were expected to be high during the high pollution event. However, the OC/EC and SOC/POC ratios were 4.96 and 0.70, 5.08 and 0.74, and 5.58 and 0.91 during the high pollution, high PM, and low pollution events, respectively. The observed discrepancy may have resulted from the NO_x levels. For example, Han and Jang (2023) [50] and Chen et al. (2022) [30] indicated that, under relatively high NO concentrations, the reaction between NO and peroxy radicals (RO_2) is the major formation process of SOA. The product of this reaction is alkoxy radicals, a highly volatile chemical species that is unconducive to the formation of SOA. As the NO_x concentration increased, the reaction between NO and RO_2 was enhanced, resulting in an SOA yield reduction.

In this study, the average NO_x concentration during the daytime was 21.6 ppb, 20.8 ppb, and 17.1 ppb during the high pollution, high PM, and low pollution events, respectively. Since the O_3 formation over Bangkok was more likely to be a volatile organic compound (VOC)-limited (or NO_x-rich) regime [51], an increase in the NO_x level tended to decrease the SOA yield, resulting in a lower SOA yield during the high pollution event and a higher SOA yield during the low pollution event.

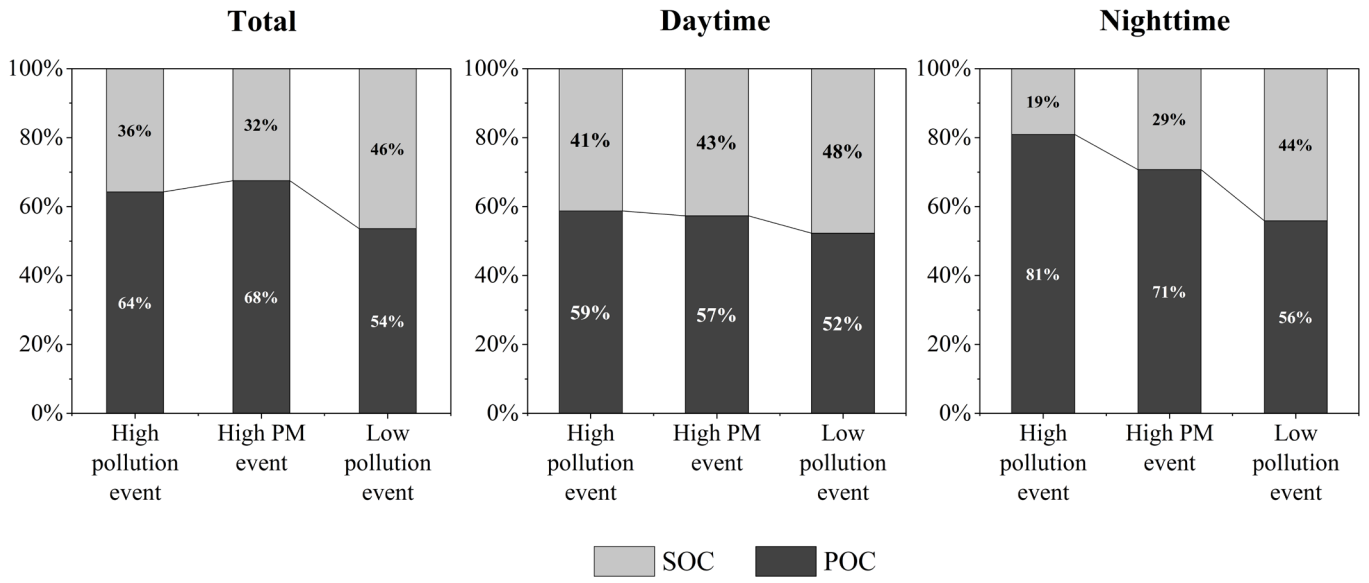

Figure 4. POC and SOC contributions to OC in the daytime and night-time during the high pollution, high PM, and low pollution events.

At night, the O_3-driven formation of SOA is suppressed due to the formation of OH radicals, and O_3 is inhibited through photochemical processes. Therefore, SOA can be formed continuously through the ozonolysis of HC and NO_3-driven oxidation [19,52–54]. At night, O_3 generated during the daytime is titrated by NO, resulting in O_3 depletion; however, the reaction is not rapid. Accordingly, O_3 can react with NO_2 to generate NO_3 radicals, and SOA formation occurs through NO_3-driven oxidation. The yield of SOA formed from this process rises with increasing NO_x [19]. Consequently, the SOC contribution to OC during the high pollution event was expected to be high due to the high concentrations of O_3 and NO_x. However, the SOC/POC ratios from our study showed the opposite result. The SOC/POC ratio was 0.44, 0.34, and 0.83 during the high pollution, high PM, and low pollution events, respectively (Table 4). The SOC contribution to OC accounted for 31%, 25%, and 45% during the high pollution, high PM, and low pollution events, respectively (Figure 4). This was because O_3 can react either with NO to generate NO_2 or with NO_2 to generate NO_3, with the latter leading to SOA formation through NO_3-driven oxidation. The NO/NO_2 ratio was calculated to evaluate the competition between the reactions of O_3 with NO and NO_2. The average NO/NO_2 ratio was 0.15, 0.20, and 0.16 during the high pollution, high PM, and low pollution events, respectively. During the high PM event, the high NO concentration could be a possible reason to retard the SOA formation through NO_3-driven oxidation. The RH level may be the cause of the differences in SOA formation between the high pollution and low pollution events since the high RH level can enhance the partitioning between the gas–particle phases of low-volatile compounds, the surface area of aerosols, and the chemistry of aqueous aerosols, thus increasing the SOA yield [55]. We found that the average RH level was lower during the high pollution event (56.83%) than during the low pollution event (57.35%). However, the reason for the difference in the SOA formation between the high pollution and low pollution events still remains unclear.

4. Conclusions

The SOC campaign was conducted in January 2021 to investigate SOA formation over Bangkok. The chemical species of OC (POC and SOC), EC, O_3, $PM_{2.5}$, and PM_{10} and meteorological factors were observed at 30 m agl at the KU tower. During the study period, the atmospheric conditions were classified as high pollution, high PM, and low pollution events. Even though this study has some limitations, including a lack of $PM_{2.5}$ chemical compositions and VOC concentration data during the study period and a short study period, the results from this study reveal the atmospheric fate and chemistry of $PM_{2.5}$ formation over Bangkok. The correlations between $PM_{2.5}$ and O_3 were negative during the three events. Negative correlations in the daytime implied that the high PM concentrations could attenuate sunlight and suppress the photochemical reactions to form O_3. The negative correlations at night-time occurred since O_3 could not be formed but was destroyed by several chemical reactions. The moderate OC/EC values implied that fossil fuel combustion (i.e., from traffic) was the major carbonaceous aerosol in Bangkok. The EC tracer-estimated SOC and POC showed that SOC contributed 32.5 to 46.4% to the OC. Most strikingly, during the low pollution event, SOC contributed approximately 50% to the OC, which revealed that SOA formation was higher during the low pollution event than during the high pollution and high PM events. The heightened formation of SOA during the low pollution event was perhaps due to the NO_x levels. Since Bangkok is more likely to have a NO_x-rich photochemical reaction regime, an increase in the NO_x level tends to decrease the SOA yield. Together with the high humidity and high light intensity during the low pollution event, the SOA formation was enhanced. Although the driving factors of SOA formation over Bangkok remain unclear, the results of this study revealed the significance and urgency of local actions to reduce NO_x and O_3 to achieve more habitable and sustainable urban environments.

Author Contributions: Conceptualization, P.U., P.C., S.B. and T.T.; Methodology, P.U., P.C., S.B. and T.T.; Formal analysis, P.U., P.C., J.P. and T.T.; Investigation, P.U., P.C., J.P. and T.T.; Visualization, P.U., P.C. and J.P.; Writing—Original Draft, P.U., P.C., J.P. and T.T.; Writing—Review and Editing, P.U., P.C., S.B. and T.T.; Supervision, S.B. All authors have read and agreed to the published version of the manuscript.

Funding: This research received no external funding.

Institutional Review Board Statement: Not applicable.

Informed Consent Statement: Not applicable.

Data Availability Statement: The data will be made available upon request.

Acknowledgments: This study was funded by the 'Atmospheric Science Research Group (ASRG)' and the Faculty of Environment, Kasetsart University, Bangkok, Thailand.

Conflicts of Interest: The authors declare no conflict of interest.

References

1. Ambient Air Quality Standard for PM2.5 Act. 139 § 163. 2022. Available online: https://ratchakitcha2.soc.go.th/pdfdownload/?id=139D163S0000000002100 (accessed on 30 June 2022).
2. Thai Meteorological Department. The Climate of Thailand. Available online: https://www.tmd.go.th/en/archive/thailand_climate.pdf (accessed on 30 June 2022).
3. Uttamang, P.; Aneja, V.P.; Hanna, A.H. Assessment of gaseous criteria pollutants in the Bangkok Metropolitan Region, Thailand. *Atmos. Chem. Phys.* **2018**, *18*, 12581–12593. [CrossRef]
4. Bangkok Metropolitan Administration. AQI Information. Available online: https://bangkokairquality.com/bma/aqi?lang=en (accessed on 14 March 2023).
5. Phairuang, W.; Hongtieab, S.; Suwattiga, P.; Furuuchi, M.; Hata, M. Atmospheric ultrafine particulate matter (PM0.1)-bound carbon composition in Bangkok, Thailand. *Atmosphere* **2022**, *13*, 1676. [CrossRef]
6. Thangavel, P.; Park, D.; Lee, Y.-C. Recent Insights into Particulate Matter ($PM_{2.5}$)-Mediated Toxicity in Humans: An Overview. *Int. J. Environ. Res. Public Health* **2022**, *19*, 7511. [CrossRef]

7. United State Environmental Protection Agency (US.EPA). Particulate Matter (PM) Pollution Health and Environmental Effects of Particulate Matter (PM). Available online: https://www.epa.gov/pm-pollution/health-and-environmental-effects-particulate-matter-pm (accessed on 14 March 2023).
8. Wetchayont, P.; Hayasaka, T.; Khatri, P. Air Quality Improvement during COVID-19 Lockdown in Bangkok Metropolitan, Thailand: Effect of the Long-range Transport of Air Pollutants. *Aerosol Air Qual. Res.* **2021**, *21*, 200662. [CrossRef]
9. Choomanee, P.; Bualert, S.; Thongyen, T.; Salao, S.; Szymanski, W.W.; Rungratanaubon, T. Vertical variation of carbonaceous aerosol with in the PM2.5 fraction in Bangkok, Thailand. *Aerosol Air Qual. Res.* **2020**, *20*, 43–52. [CrossRef]
10. Rattanapotanan, T.; Thongyen, T.; Bualert, S.; Choomanee, P.; Suwattiga, P.; Rungrattanaubon, T.; Utavong, T.; Phupijit, J.; Changplaiy, N. Secondary source of PM2.5 based on the vertical distribution of organic carbon, elemental carbon, and water-soluble ions in Bangkok. *Environ. Adv.* **2023**, *11*, 100337. [CrossRef]
11. Zhang, H.-H.; Li, Z.; Liu, Y.; Xinag, P.; Cui, X.-Y.; Ye, H.; Hu, B.-I.; Lou, L.-P. Physical and chemical characteristics of $PM_{2.5}$ and its toxicity to human bronchial cells BEAS-2B in the winter and summer. *J. Zhejiang Univ. Sci. B* **2018**, *19*, 317–326. [CrossRef]
12. Pani, S.K.; Lin, N.-H.; Chantra, S.; Wang, S.-H.; Khamlkaew, C.; Prapamontol, T.; Janjai, S. Radiative response of biomass-burning aerosols over an urban atmosphere in northern peninsular Southeast Asia. *Sci. Total Environ.* **2018**, *633*, 892–911. [CrossRef]
13. Yoo, H.Y.; Kim, K.A.; Kim, Y.P.; Jung, C.H.; Shin, H.J.; Moon, K.J.; Park, S.M.; Lee, J.Y. Validation of SOC Estimation using OC and EC Concentration in $PM_{2.5}$ Measured at Seoul. *Aerosol Air Qual. Res.* **2022**, *22*, 210388. [CrossRef]
14. Turpin, B.J.; Huntzicker, J.J. Secondary formation of organic aerosol in the Los Angeles basin: A descriptive analysis of organic and elemental carbon concentrations. *Atmos. Environ.* **1991**, *24A*, 207–215. [CrossRef]
15. Day, M.C.; Zhang, M.; Pandis, S.N. Evaluation of the ability of the EC tracer method to estimate secondary organic carbon. *Atmos. Environ.* **2015**, *112*, 317–325. [CrossRef]
16. Kaskaoutis, D.G.; Grivas, G.; Theodosi, C.; Tsagkaraki, M.; Paraskevopoulou, D.; Stavroulas, I.; Liakakou, E.; Gkikas, A.; Hatzianastassiou, N.; Wu, C.; et al. Carbonaceous Aerosols in Contrasting Atmospheric Environments in Greek Cities: Evaluation of the EC-tracer Methods for Secondary Organic Carbon Estimation. *Atmosphere* **2020**, *11*, 161. [CrossRef]
17. Lim, H.-J.; Turpin, B.J. Origins of primary and secondary organic aerosol in Atlanta: Results of time-resolved measurements during the Atlanta Supersite Experiment. *Environ. Sci. Technol.* **2002**, *36*, 4489–4496. [CrossRef]
18. Salma, I.; Varga, P.T.; Vasanits, A.; Machon, A. Secondary organic carbon in different atmospheric environments of a continental region and seasons. *Atmos. Res.* **2022**, *278*, 106360. [CrossRef]
19. Han, S.; Jang, M. Modeling daytime and nighttime secondary organic aerosol formation via multiphase reactions of biogenic hydrocarbons. *ACP* **2023**, *23*, 1209–1226. [CrossRef]
20. Jia, M.; Zhao, T.; Cheng, X.; Gong, S.; Zhang, X.; Tang, L.; Liu, D.; Wu, X.; Wang, L.; Chen, Y. Inverse relations of $PM_{2.5}$ and O_3 in air compound pollution between cold and hot seasons over an urban area of east China. *Atmosphere* **2017**, *8*, 59. [CrossRef]
21. Zhu, J.; Chen, L.; Liao, H.; Dang, R. Correlations between $PM_{2.5}$ and Ozone over China and Associated Underlying Reasons. *Atmosphere* **2019**, *10*, 352. [CrossRef]
22. Feng, T.; Zhao, S.; Bei, N.; Wu, J.; Liu, S.; Li, X.; Liu, L.; Qian, Y.; Yang, Q.; Wang, Y.; et al. Secondary organic aerosol enhanced by increasing atmospheric oxidizing capacity in Beijing–Tianjin–Hebei (BTH), China. *Atmos. Chem. Phys.* **2019**, *19*, 7429–7443. [CrossRef]
23. Liu, Y.; Zhao, Q.; Hao, X.; Zhao, J.; Zhang, Y.; Yang, X.; Fu, Q.; Xu, X.; Wang, X.; Huo, J.; et al. Increasing surface ozone and enhanced secondary organic carbon formation at a city junction site: An epitome of the Yangtze River Delta, China (2014–2017). *Environ. Pollut.* **2020**, *265*, 114847. [CrossRef]
24. Li, K.; Jacob, D.J.; Liao, H.; Shen, L.; Zhang, Q.; Bates, K.H. Anthropogenic drivers of 2013–2017 trends in summer surface ozone in China. *Proc. Natl. Acad. Sci. USA* **2019**, *116*, 422–427. [CrossRef]
25. Fan, H.; Zhao, C.; Yang, Y.; Yang, X. Spatio-Temporal Variations of the $PM_{2.5}/PM_{10}$ Ratios and Its Application to Air Pollution Type Classification in China. *Front. Environ. Sci.* **2021**, *9*, 692440. [CrossRef]
26. Franzin, B.T.; Guizellini, F.C.; de Babos, D.V.; Hojo, O.; Pastre, I.A.; Marchi, M.R.R. Characterization of Atmospheric Aerosol (PM_{10} and $PM_{2.5}$) from a Medium Sized City in São Paulo State, Brazil. *J. Environ. Sci.* **2020**, *89*, 238–251. [CrossRef]
27. Spandana, B.; Rao, S.S.; Upadhya, A.R.; Kulkarni, P.; Sreekanth, V. PM2.5/PM10 ratio characteristics over urban sites of India. *Adv. Space Res.* **2021**, *67*, 3134–3146. [CrossRef]
28. Xu, G.; Jiao, L.; Zhang, B.; Zhao, S.; Yuan, M.; Gu, Y.; Liu, J.; Tang, X. Spatial and Temporal Variability of the $PM_{2.5}/PM_{10}$ Ratio in Wuhan, Central China. *Aerosol Air Qual. Res.* **2017**, *17*, 741–751. [CrossRef]
29. Zhao, D.; Chen, H.; Yu, E.; Luo, T. PM2.5/PM10 Ratios in Eight Economic Regions and Their Relationship with Meteorology in China. *Adv. Meteorol.* **2019**, *2019*, 5295726. [CrossRef]
30. Chen, Y.J.; Zhi, G.R.; Feng, Y.L.; Fu, J.M.; Feng, J.L.; Sheng, G.Y.; Simoneit, B.R.T. Measurements of emission factors for primary carbonaceous particles from residential raw-coal combustion in China. *Geophys. Res. Lett.* **2006**, *33*, 382. [CrossRef]
31. Chow, J.C.; Watson, J.G.; Chen, L.W.A.; Arnott, W.P.A.; Moosmüller, H.; Fung, K. Equivalence of elemental carbon by thermal/optical reflectance and transmittance with different temperature protocols. *Environ. Sci. Technol.* **2004**, *38*, 4414–4422. [CrossRef]
32. He, L.Y.; Hu, M.; Huang, X.F.; Yu, B.D.; Zhang, Y.H.; Liu, D.Q. Measurement of emissions of fine particulate organic matter from Chinese cooking. *Atmos. Environ.* **2004**, *38*, 6557–6564. [CrossRef]

33. Zhang, Y.X.; Shao, M.; Zhang, Y.H.; Zeng, L.M.; He, L.Y.; Zhu, B.; Wei, Y.J.; Zhu, X.L. Source profiles of particulate organic matters emitted from cereal straw burnings. *J. Environ. Sci.* **2007**, *19*, 167–175. [CrossRef]
34. Qi, M.; Jiang, L.; Liu, Y.; Xiong, Q.; Sun, C.; Li, X.; Zhao, W.; Yang, X. Analysis of the characteristics and sources of carbonaceous aerosols in $PM_{2.5}$ in the Beijing, Tianjin, and Langfang Region, China. *Int. J. Environ. Res. Public Health* **2018**, *15*, 1483. [CrossRef]
35. Department of Land Transport. Nation Transportation Statistics. Available online: https://web.dlt.go.th/statistics/index.php (accessed on 30 November 2022).
36. Phairuang, W.; Inerb, M.; Furuuchi, M.; Hata, M.; Tekasakul, S.; Tekasakul, P. Size-fractionated carbonaceous aerosols down to PM0.1 in southern Thailand: Local and long-range transport effects. *Environ. Pollut.* **2020**, *260*, 114031. [CrossRef] [PubMed]
37. Aman, N.; Manomaiphiboon, K.; Suwattiga, P.; Assareh, N.; Limpaseni, W.; Suwanathada, P.; Soonsin, V.; Wang, Y. Visibility, aerosol optical depth, and low-visibility events in Bangkok during the dry season and associated local weather and synoptic patterns. *Environ. Monit. Assess.* **2022**, *194*, 322. [CrossRef] [PubMed]
38. Chow, J.C.; Watson, J.G.; Chen, W.A.; Chang, M.O.; Robinson, N.F.; Trimble, D.; Kohl, S. The IMPROVE_A temperature protocol for thermal/optical carbon analysis: Maintaining consistency with a long-term database. *J. Air Waste Manag. Assoc.* **2012**, *57*, 1014–1023. [CrossRef]
39. Han, Y.M.; Cao, J.J.; Chow, J.C.; Watson, J.G.; An, Z.; Jin, Z.S.; Fung, K.; Liu, S. Evaluation of the thermal/optical reflectance method for discrimination between char- and soot-EC. *Chemosphere* **2007**, *69*, 569–574. [CrossRef]
40. Karanasiou, A.; Minguilloón, M.C.; Viana, M.; Alastuey, A.; Putaud, J.P.; Maenhaut, W.; Pantelladis, P.; Močnik, G.; Favez, O.; Kuhlbusch, T.A.J. Thermal-optical analysis for the measurement of elemental carbon (EC) and organic carbon (OC) in ambient air a literature review. *Atmos. Meas. Technol.* **2015**, *8*, 9649–9712.
41. Bautista VII, A.T.; Pabroa, P.C.B.; Santos, F.L.; Quirit, L.L.; Asis, J.L.B.; Dy, M.A.K.; Martinez, J.P.G. Intercomparison between NIOSH, IMPROVE_A, and EUSAAR_2 protocols: Finding an optimal thermal– optical protocol for Philippines OC/EC samples. *Atmos. Pollut. Res.* **2015**, *6*, 334–342. [CrossRef]
42. Srivastava, D.; Daellenbach, K.R.; Zhang, Y.; Bonnaire, N.; Chazeau, B.; Perraudin, E.; Gros, V.; Lucarelli, F.; Villenave, E.; Prévôt, A.S.H.; et al. Comparison of five methodologies to apportion organic aerosol sources during a PM pollution event. *Sci. Total Environ.* **2021**, *757*, 143168. [CrossRef]
43. Wu, C.; Wu, D.; Yu, J.Z. Estimation and Uncertainty Analysis of Secondary Organic Carbon Using 1 Year of Hourly Organic and Elemental Carbon Data. Journal of Geophysical Research. *Atmospheres* **2019**, *124*, 2774–2795.
44. Coa, J.J.; Zhu, C.S.; Tie, X.X.; Geng, F.H.; Ho, S.S.H.; Wang, G.H.; Han, Y.M.; Ho, K.F. Characteristics and sources of carbonaceous aerosols from Shanghai, China. *Atmos. Chem. Phys.* **2013**, *13*, 803–817.
45. Tiwari, S.; Dumka, U.C.; Kaskaoutis, D.G.; Ram, K.; Panicker, A.S.; Srivastava, M.K.; Tiwari, S.; Attri, S.D.; Soni, V.K.; Pandey, A.K. Aerosol chemical characterization and role of carbonaceous aerosol on radiative effect over Varanasi in central Indo-Gangetic Plain. *Atmos. Environ.* **2016**, *125*, 437–449. [CrossRef]
46. Wu, C.; Yu, J.Z. Determination of primary combustion source organic carbon-to-elemental carbon (OC /EC) ratio using ambient OC and EC measurements: Secondary OC-EC correlation minimization method. *Atmos. Chem. Phys.* **2016**, *16*, 5453–5465. [CrossRef]
47. Zhang, H.; Wang, Y.; Hu, J.; Ying, Q.; Hu, X.-M. Relationships between meteorological parameters and criteria air pollutants in three megacities in China. *Environ. Res.* **2015**, *140*, 242–254. [CrossRef]
48. Devi, N.L.; Kumar, A.; Yadav, I.C. PM10 and PM2.5 in Indo-Gangetic Plain (IGP) of India: Chemical characterization, source analysis, and transport pathways. *Urban Clim.* **2020**, *33*, 100663. [CrossRef]
49. Dumka, U.C.; Tiwari, S.; Kaskaoutis, D.G.; Hopke, P.K.; Singh, J.; Srivastava, A.K.; Bisht, D.S.; Attri, S.D.; Tyagi, S.; Misra, A.; et al. Assessment of PM2.5 chemical compositions in Delhi: Primary vs. secondary emissions and contribution to light extinction coefficient and visibility degradation. *J. Atmos. Chem.* **2017**, *74*, 423–450. [CrossRef]
50. Han, S.; Bian, H.; Feng, Y.; Liu, A.; Li, X.; Zeng, F.; Zhang, X. Analysis of the Relationship between O_3, NO and NO_2 in Tianjin, China. *Aerosol Air Qual. Res.* **2011**, *11*, 128–139. [CrossRef]
51. Uttamang, P.; Campbell, P.C.; Aneja, V.P.; Hanna, A.F. A multi-scale model analysis of ozone formation in the Bangkok Metropolitan Region, Thailand. *Atmos. Environ.* **2020**, *229*, 117433. [CrossRef]
52. Gaoa, S.; Lathem, T.; Nyadong, L. Nighttime secondary organic aerosol formation from unburned fuel vapors. *Atmos. Environ.* **2019**, *204*, 125–134. [CrossRef]
53. Palm, B.B.; Campuzano-Jost, P.; Day, D.A.; Ortega, A.M.; Fry, J.L.; Brown, S.S.; Zarzana, K.J.; Dube, W.; Wagner, N.L.; Draper, D.C.; et al. Secondary organic aerosol formation from in situ OH, O_3, and NO_3 oxidation of ambient forest air in an oxidation flow reactor. *Atmos. Chem. Phys.* **2017**, *17*, 5331–5354. [CrossRef]
54. Zaveri, R.A.; Shilling, J.E.; Fast, J.D.; Springston, S.R. Efficient nighttime biogenic SOA formation in a polluted residual layer. *J. Geophys. Res. Atmos.* **2020**, *125*, e2019JD031583. [CrossRef]
55. Jiang, X.; Tsona, N.T.; Jia, L.; Liu, S.; Zhang, H.; Xu, Y.; Du, L. Secondary organic aerosol formation from photooxidation of furan: Effects of NOx and humidity. *Atmos. Chem. Phys.* **2019**, *19*, 13591–13609. [CrossRef]